Journal of Electroceramics, 15, 159–166, 2005


# The Effect of Cobalt Oxide Addition on the Conductivity of $Ce_{0.9}Gd_{0.1}O_{1.95}$

EVA JUD* & LUDWIG J. GAUCKLER

*Institute of Nonmetallic Inorganic Materials, Department of Materials, Swiss Federal Institute of Technology, ETH Zurich, CH-8093 Zurich, Switzerland*

Submitted December 9, 2004; Revised April 1, 2005

**Abstract.** The conductivity of cobalt oxide doped $Ce_{0.9}Gd_{0.1}O_{1.95}$ (CGO10) of various doping concentrations, sintering temperatures, dwell times, and cooling rates was investigated by 4-point DC conductivity measurements. In cobalt oxide doped CGO10, an enhanced total conductivity occuring with a low activation energy of 0.54 eV was detected below 250°C in quenched samples. If the same samples were cooled down slowly, only the ionic conductivity of undoped CGO with an activation energy of 0.8 eV was found. The increased conductivity is attributed to a percolating network of an electronically conducting grain boundary phase rich in CoO, which can be retained by quenching from temperatures between 900 and 1000°C.

**Keywords:** ceria solid solution, cobalt oxide, mixed ionic electronic conductivity, grain boundary segregation

## Introduction

It is a long-standing objective of Solid Oxide Fuel Cells (SOFC) technology to reduce the cost of operation as well as that of production. Progress towards lower cost depends in the first place on reducing the operation temperature of 950°C without losing efficiency. Lower operation temperatures promise the use of less expensive materials for interconnector and insulation components in the construction of SOFCs. The key to maintain high efficiency at temperatures around 600–700°C lies in reducing the electrolyte thickness [1] or in replacing the currently standard solid electrolyte, yttria-stabilized zirconia, by a material with higher oxygen ion conductivity at these lower temperatures [2]. Ceria solid solutions are considered the most suitable alternative electrolyte materials [3, 4]. In particular, $Ce_{1-x}Gd_xO_{2-x/2}$ electrolytes possess a high ionic conductivity as shown in various studies [5–11]. Sintering $Ce_{1-x}Gd_xO_{2-x/2}$ ceramics to relative densities >95% (i.e. closed porosity) requires temperatures >1300°C resulting in micron-sized microstructures with poor mechanical properties [12–14]. The use of transition metal oxides (e.g. cobalt oxide) as sintering aid for $Ce_{0.8}Gd_{0.2}O_{1.9}$ (CGO20) and $Ce_{0.9}Gd_{0.1}O_{1.95}$ (CGO10) leads to grain sizes in the sub-micron range (∼120 nm) with possible improved mechanical stability [15–17]. It was further shown that 2 cat% cobalt oxide represents the most appropriate doping concentration and increases the sintering rate, so that dense microstructures are achieved already at 900°C. Kleinlogel et al. argued that the improved sintering characteristics are due to an approximately 2 nm thick amorphous cobalt rich grain boundary phase, which disappears at higher sintering temperature and/or with increasing dwell time [15, 17]. Based on impedance spectroscopy, they concluded that cobalt oxide dissolves into the CGO lattice. Compared to undoped CGO20, the oxygen ion conductivity was found to be unchanged in equilibrated cobalt oxide doped samples. However, electronic conductivity along the cobalt rich grain boundary layers was detected in material sintered for short time. Later, Lewis et al. reported that cobalt oxide remains at the grain boundaries of CGO10 after a holding time of 12 h at 980°C Lewis et al. [18]. It was suggested that cobalt oxide does not entirely wet the CGO grains, which renders the detection of

*To whom all correspondence should be addressed. E-mail: eva.jud@mat.ethz.ch

cobalt oxide at the boundaries difficult. Furthermore, they measured a higher lattice conductivity in 2 cat% doped CGO and explained this by the formation of additional oxygen vacancies due to the substitution of $Co^{3+}$ for $Ce^{4+}$ resulting in a minimum lattice parameter change. The electrical properties of cobalt oxide doped CGO20 were also investigated by Fagg et al. [19]. They found that the total electrical conductivity remains unchanged when 2 cat% of cobalt oxide is added as long as sintering is performed at 900 to 1000°C. In doped samples, increased *p*-type conductivity was detected and a decrease of the oxygen ion transference number from 0.99 to 0.89 was determined between 650 and 1000°C. Also, the existence of enriched cobalt oxide boundary layers was confirmed for CGO20 samples at 900°C, but distinct areas of higher cobalt oxide concentration were detected as well.

The results of [17–19] show that the exact role of cobalt oxide as sintering aid for CGO is not understood yet. The mechanism of action of cobalt oxide is probably more complex than that of a simple liquid phase additive as previously suggested [15, 16].

Our recent sintering and grain growth studies of cobalt oxide doped CGO20 suggested that cobalt oxide doping acts as an activator material [20, 21]. Activated sintering has extensively been described for the case of $Bi_2O_3$-doped ZnO and manifests itself mainly in increased shrinkage rates below the eutectic temperature combined with intergranular films [22]. However, for the application of cobalt oxide doped CGO electrolytes, it is crucial to understand the influence of cobalt oxide doping onto the conductivity and microstructure of CGO. With a detailed understanding, the appropriate doping level and sintering cycle for optimal electrical performance of the electrolyte material and hence of the SOFC can be developed. This study aims at elucidating the electrical properties of the cobalt oxide rich grain boundary layer in CGO in more detail. By choosing suitable sintering temperatures and especially variable cooling rates, the relationship between conductivity and microstructure of cobalt oxide doped CGO is investigated.

## Experimental Procedures

$Ce_{0.9}Gd_{0.1}O_{1.95}$ (CGO10) powder was supplied by Rhodia Electronics & Catalysis. Powder particle sizes were characterized by BET measurements (Nova1000, Quantachrome) and *X*-ray diffraction (XRD-Diffractometer D 5000, Siemens) combined with Rietveld refinement (TOPAS R 2.0, Bruker AXS). The CGO10 powder was doped with cobalt oxide by ultrasonic dispersion in ethanol for 10 min and by addition of the desired amount of cobalt nitrate hexahydrate (Fluka Chemie AG) dissolved in ethanol. The suspension consisting of powder and cobalt was subsequently dispersed for another 10 min, dried at 120°C and ground in an agate mortar. Calcination at 400°C for 2 h decomposed the cobalt nitrate to cobalt oxide followed by a second grinding step in an agate mortar. Green bodies were obtained by first uniaxial pressing of 4 g of powders and subsequent isostatic pressing at 300 MPa for 3 min that yielded test bars of $30*4*4$ mm (length * width * height). The sample bars were sintered at 900 and 1000°C for various dwell times and either quenched in air or slowly cooled (−0.5°C/min). Grain sizes were estimated from fracture surfaces imaged by scanning electron microscopy (LEO 1530). A grain intersection to grain size conversion factor of 1.56 was used [23]. The Si impurity content was determined by laser ablation with a spot size of 30 $\mu$m combined with inductively coupled plasma mass spectroscopy [24].

Contacts for DC 4-point conductivity measurements were made by wrapping a platinum wire around the sintered bars and by applying a platinum paste (C 3605 P, Heraeus GmbH). The bars were then heated to 330°C for 15 min in order remove the organics of the platinum paste. The annealing temperature of 330°C was chosen above the decomposition temperature of the organic components of the platinum paste, which had previously been determined by a differential thermal and thermogravimetric analysis DTA/TG (STA 501, Bähr Thermoanalyse AG) at a heating rate of 10°C/min. Finally, the platinum wire leads were fixed to the contact patches with a ceramic two component binder. Resistance measurements were taken with a multimeter (197A, Keithley) during heating and cooling (±3°C/min) up to 900°C. For the HRTEM analysis, samples were prepared by first grinding, dimpling, polishing and finally ion milling in a Gatan Duomill. For ion milling, an inclination angle of 12° and an Ar ion energy in the range of 2.5–4 keV was used. The JEOL ARM 1250 microscope with a point-to point-resolution of 0.12 nm was used for the HRTEM studies. The microscope is equipped with a drift compensation system, which helps stabilizing the image. Bright field images were obtained on a Tecnai F30 microscope (FEI) with a field emission gun operated at 300 kV. Elemental

*Table 1.* Average grain size and conductivity of CGO10 sintered at 1200 and 1400°C.

| $T$ | $G$ | $\rho$ | Conductivity $T < 400$°C | Conductivity $T > 400$°C |
|---|---|---|---|---|
| 1200°C | 0.54 $\mu$m | 90% | $\sigma T = 1.47 \cdot 10^6 \exp(\frac{0.87\ \text{eV}}{k_B T}) \frac{S \cdot K}{\text{cm}}$ | $\sigma T = 1.81 \cdot 10^5 \exp(\frac{0.73\ \text{eV}}{k_B T}) \frac{S \cdot K}{\text{cm}}$ |
| 1400°C | 0.92 $\mu$m | 98% | $\sigma T = 5.25 \cdot 10^5 \exp(\frac{0.81\ \text{eV}}{k_B T}) \frac{S \cdot K}{\text{cm}}$ | $\sigma T = 1.49 \cdot 10^5 \exp(\frac{0.72\ \text{eV}}{k_B T}) \frac{S \cdot K}{\text{cm}}$ |

mappings were obtained by electron spectroscopic imaging (three window technique) using an imaging filter (GIF, Gatan) mounted below the microscope column. Samples were prepared by crushing and dispersing them onto holey carbon films supported on copper grids.

## Results and Discussion

The total conductivity data of undoped CGO10 as a function of reciprocal temperature are plotted for two sintering temperatures in Fig. 1. In general, the total conductivity can be represented by

$$\sigma T = \sigma_0 T \exp\left(\frac{-E_a}{k_B T}\right) \tag{1}$$

Here, $\sigma$ is the measured total conductivity, $\sigma_0$ is a pre-exponential term, $E_a$ is the activation energy, $k_B$ the Boltzmann constant and $T$ the absolute temperature. The conductivity curves of CGO10 sintered at 1200

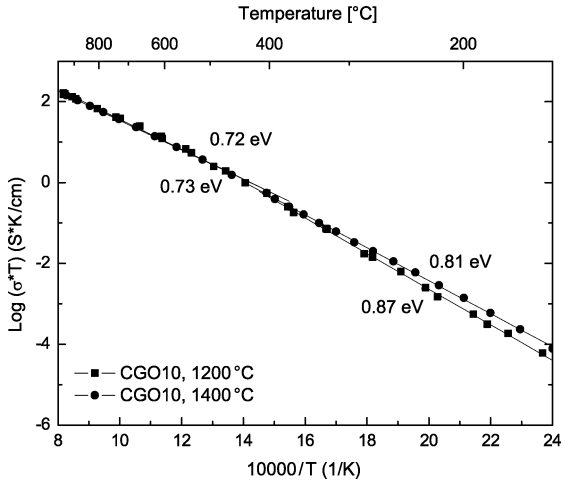


*Fig. 1.* Electrical conductivity of CGO10 sintered at 1200 and 1400°C as a function of temperature.

and 1400°C in Fig. 10 show a change in slope at around 400°C. The measured conductivity can reasonably described with the expressions as shown in Table 1. Surprisingly, a few percent of porosity did not influence the total conductivity since the sample sintered at 1200°C exhibited only a density of 90% whereas the sample sintered at 1400°C was 98% dense. Gerhardt et al. reported a decrease in lattice and grain boundary conductivity of $Ce_{0.94}Gd_{0.06}O_{2-x}$ due to a lower relative density [25]. Based on their data, the decrease in conductivity can be estimated to be roughly 8% for a density reduction from 95% to 70%. In this work, the difference in density is much smaller, and the total conductivity remains unchanged, which is consistent with the above estimate. The activation energy at temperatures above 400°C does not change with the sintering temperature and the average grain size. At temperatures below 400°C, the sample sintered at 1400°C shows a slightly higher total conductivity combined with a lower activation energy. It is inferred that the higher activation energy and lower total conductivity at $T < 400$°C is due to the larger grain boundary area and consequently the higher grain boundary resistivity of the 1200°C sample. Zhou et al. have shown that grain boundary resistivity in CGO10 becomes neglectable at temperatures >600°C [26]. The effect of grain size can therefore only be detected at low temperatures. The herein reported values of the absolute activation energies of the sample sintered at 1400°C are larger than those of [4]. although he used the same starting powder and the same sintering temperature, i.e. 1400°C. This observation points at the presence of certain impurities that artifically increase the activation energy. $SiO_2$ is known to be the main impurity found in the grain boundary region of ceria-based materials. The average Si content in a CGO10 sample sintered in a dedicated clean alumina furnace was found to be $233 \pm 20$ ppm. According to the supplier of the presently used powder, the maximum $SiO_2$ content is below 100 ppm. Although precautions have been taken to avoid contamination during the preparative steps of the experiments, the measured amount of Si in the investigated samples may influence the total conductivity.

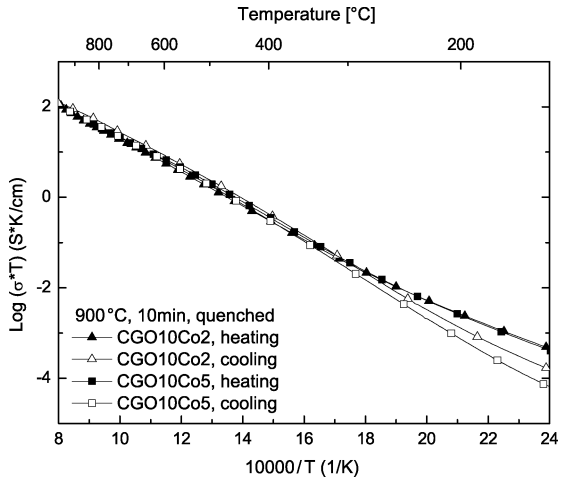


*Fig. 2.* Electrical conductivity of 2 and 5 cat% cobalt oxide doped CGO10 as a function of temperature. Samples were sintered at 900°C for 10 min and quenched in air.

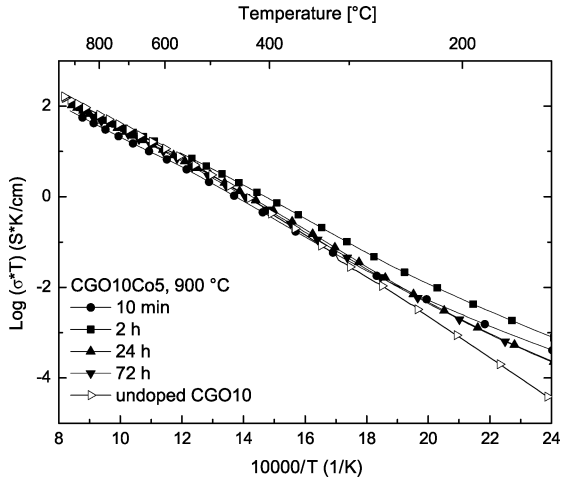


*Fig. 3.* Electrical conductivity of CGO10 doped with 5 cat% of cobalt oxide. Data was obtained during first heating after sintering at 900°C for dwell times from 10 min up to 72 h. Samples have been quenched in air.

The addition of cobalt oxide clearly changes the total conductivity of CGO10 as is visible in Fig. 2. Samples of different doping levels (2 cat% and 5 cat%) have been sintered to 900°C for 10 min and air-quenched. One notes that 900°C is also the temperature where cobalt oxide doped CGO reaches full density as was found from separate dilatometric measurements [27]. Obviously, the samples are not in equilibrium after quenching since an increased total conductivity is observed during the first heating up to approximately 250°C. During subsequent cooling, a different slope, corresponding to the conductivity of undoped CGO10, is observed. In a second heating cycle up to 900°C, only the ionic conductivity of pure CGO10 is measured. These results are consistent with those of Kleinlogel et al. [28], who reported a higher conductivity of cobalt oxide doped CGO20 compared to undoped CGO20 if measured at low temperatures. This increased total conductivity at temperatures <250°C is also observed for samples with dwell times up to 72 h at 900°C (Fig. 3) and up to 4 h at 1000°C (Fig. 4). For clarity, only the first heating cycle of the DC 4-point conductivity measurement is depicted in both Figs. 3 and 4. Similar to the data shown in Fig. 2, the cooling curve corresponds to the one of undoped CGO10. Much longer dwell times than 4 h at 1000°C produced very brittle samples not suitable for contacting. It is interesting to notice that the highest total conductivity during first heating is observed for a dwell time of 2 h.

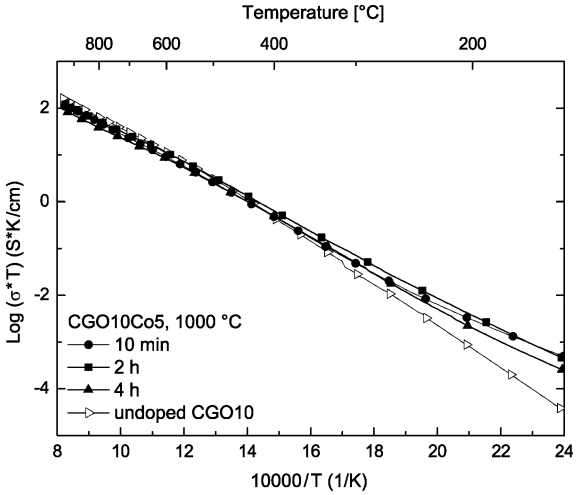


*Fig. 4.* Electrical conductivity of CGO10 doped with 5 cat% of cobalt oxide. Data was obtained during first heating after sintering at 1000°C for dwell times from 10 min up to 4 h. Samples have been quenched in air.

The increased total conductivity in cobalt oxide doped samples occurs jointly with a lower activation energy. The values of the activation energy are shown in Fig. 5. They were calculated for data taken during heating up to 250°C or during cooling from 900°C to room temperature. Most important, the activation energy during heating clearly lies below 0.6 eV whereas during

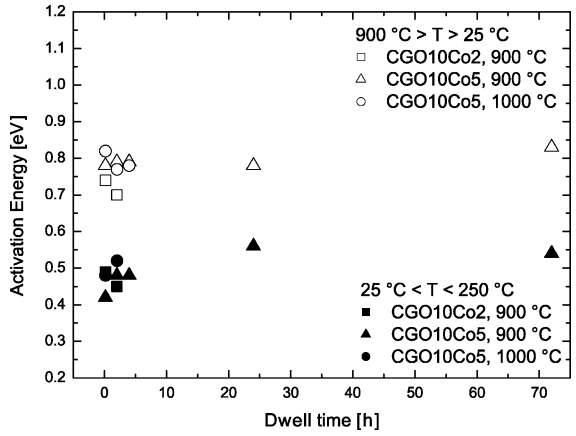


*Fig. 5.* Activation energy as a function of dwell time for samples doped with 2 and 5 cat% of cobalt oxide. All samples have been quenched in air.

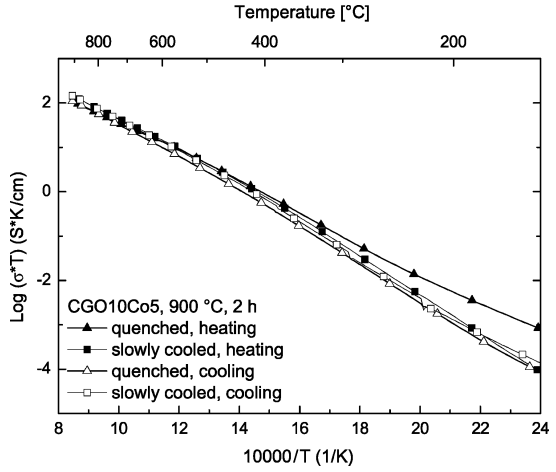


*Fig. 6.* Electrical conductivity of CGO10 doped with 5 cat% of cobalt oxide. Data was obtained during first heating after sintering at 900°C for 2 h.

cooling, values around 0.8 eV are found. Furthermore, for the 5 cat% doped samples, a slight increase in activation energy during prolonged heating is observed. Hence, the addition of cobalt oxide seems to be responsible for a second conductivity mechanism, which develops at temperatures between 900 and 1000°C.

The presence of an additional conductivity mechanism that is observable at low temperature becomes more evident by comparing a quenched to a slowly cooled sample (Fig. 6). A sample, sintered at 900°C for 2 h, but cooled with −0.5°C/min does not exhibit a second conductivity mechanism during the first heating cycle, but solely the ionic conductivity of CGO10. Further evidence is attained by observing that the high temperature state and consequently the additional conductivity mechanism can be reestablished by reheating a slowly cooled sample and quenching from 900°C. It can therefore be concluded that the additional conductivity mechanism in cobalt oxide doped CGO10 is a high temperature characteristic which can be frozen in by quenching. For an explanation, it is referred to the fact that cobalt oxide undergoes an endothermic reaction at around 900°C as $Co_3O_4$ is reduced to CoO upon heating (see for example Mocala et al. [29]). The fact that the transformation temperature of $Co_3O_4$ coincides with the maximum shrinkage rate of cobalt oxide doped CGO suggests that the reduction of $Co^{3+}$ to $Co^{2+}$ is responsible for the enhanced sintering properties [16, 18]. The existence of a high temperature conductivity mechanism as shown in the present work seems also be caused by the reduction of cobalt ions. In order to corroborate this hypothesis, already densified, doped samples were treated to specifically produce CoO or $Co_3O_4$ and their total conductivity was measured (Fig. 7). Separately, the structure of cobalt oxide was determined by weight change with DTA/TG measurements (Fig. 8).

The first sample, which was heated in air to 800°C for 4 hrs to prevent reduction of $Co_3O_4$ exhibited solely the ionic conductivity of pure CGO10. In contrast, the second sample, heated in nitrogen to 1000°C for 4 hrs to reduce $Co_3O_4$ to CoO, showed the enhanced total conductivity at low temperatures seen before. Again, an activation energy of 0.55 eV was calculated in this case.

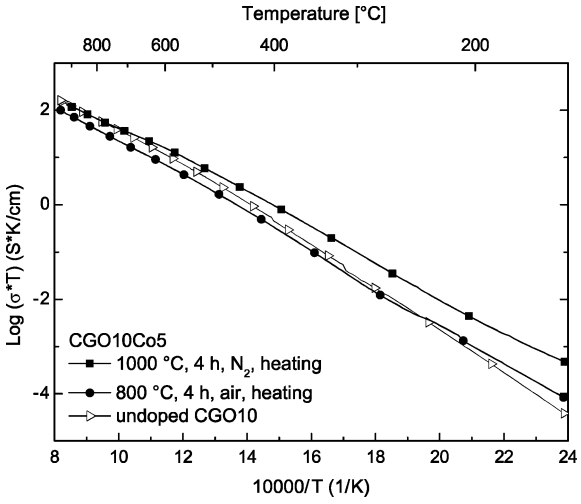


*Fig. 7.* Electrical conductivity of CGO10 doped with 5 cat% of cobalt oxide measured during heating to 900°C.

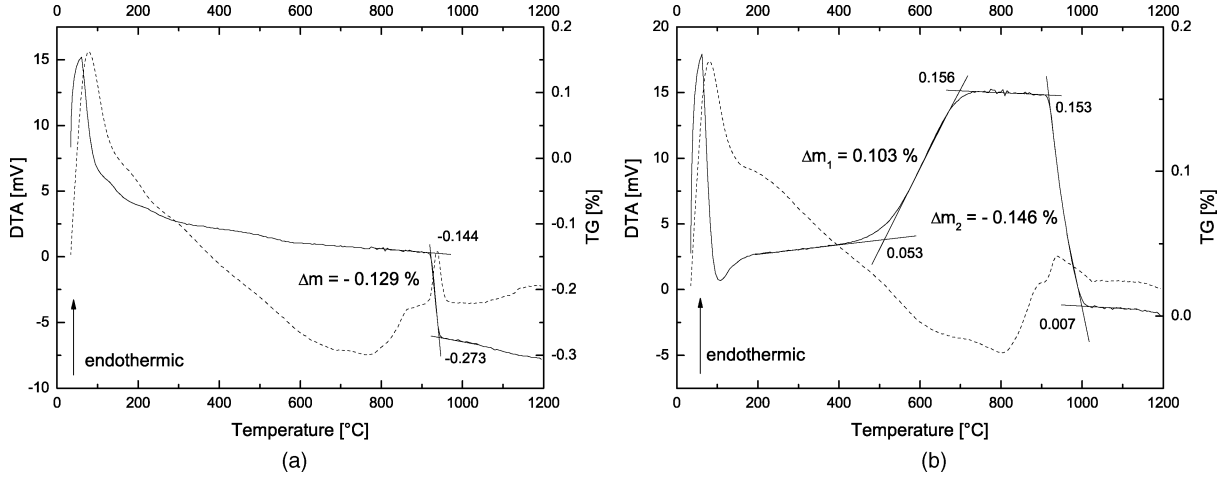


*Fig. 8.* DTA/TG analysis of CGO10 + 5 cat% cobalt oxide. Sample (a) was sintered at 800°C for 4 h in air and cooled to room temperature with 0.5°C/min. Sample (b) was sintered at 1000°C for 4 h in $N_2$ and cooled to room temperature with 2°C/min. Dashed lines represent DTA curves, solid lines represent TG curves.

The DTA/TG curve of the sample sintered at 800°C clearly showed an endothermic peak at 935°C corresponding to the transformation of $Co_3O_4$ to CoO. The measured weight loss of 0.13% corresponds to 85% of the theoretical weight loss for this transformation. In case of the sample held at 1000°C, a weight increase of 0.1% is observed during heating up to 710°C followed by a weight loss of 0.15% combined with an endothermic peak at 934°C. The weight gain during heating is assigned to the reoxidation of CoO. The weight loss of 0.15% corresponds to 97% of the theoretical loss indicating that the transformation from $Co_3O_4$ to CoO was complete within the accuracy of the measurement. Based on the DTA/TG measurements, it can therefore be concluded that the cobalt oxide phase in the sample heated to 800°C contained 85% of the total cobalt oxide as $Co_3O_4$ whereas the sample heated to 1000°C contained 68% (0.1% weight increase) of CoO. The increased conductivity at low temperatures as shown in Fig. 7 is therefore attributed to the existence and effect of $Co^{2+}$ ions in the sample. One might argue that the additional conductivity mechanism evident at low temperature may be due to electronic conductivity associated with reduced cerium ions ($Ce^{4+} \rightarrow Ce^{3+}$). This conjecture however could be excluded. An undoped CGO10 sample held at 900°C for 2 h and air-quenched did not show an increased total conductivity at low temperature.

Previous studies have already indicated that the cobalt oxide dopant is mainly located at the grain boundaries [21, 28], but also as isolated particles in the microstructure [18]. These observations could now be confirmed for the samples sintered at 900°C for 2 h, whose conductivity measurements are plotted in Fig. 6. The TEM images a) and b) in Fig. 9 represent a typical distribution of cobalt oxide particles between 20 and 500 nm in size in the CGO10 matrix and clearly demonstrate their inhomogeneous distribution. Cobalt oxide is also found at the grain boundaries in form of a thin layer of roughly 0.5 nm thickness as image c) in Fig. 9 shows. The evidence of Co at the grain boundaries has been obtained by electron energy loss spectroscopy and can be found elsewhere [30]. The thickness of the cobalt rich grain boundary film is much smaller than previously reported [17]. Furthermore, it can be assumed that only a small amount of cobalt is dissolved in the CGO10 matrix. The solubility of cobalt in $CeO_2$ has been determined to be approximately 3 mol% at 1580°C Chen et al. [31]. Similarly, the maximum solubility of cobalt in $Gd_2O_3$ is less than 2.5 mol% at around 1550°C [32]. It can therefore be estimated that less than 0.5 mol% of cobalt diffuses into CGO10 at a temperature of 900°C. This conclusion is in contrast to the results reported by Kleinlogel et al. [28], who claims that Co diffuses into the matrix at high temperatures and/or long dwell times until the amorphous grain boundary film vanishes.

A cobalt oxide rich interfacial layer present at the grain boundaries implies a percolating network. The additional conductivity measured below 250°C originates from this network of electronically conducting

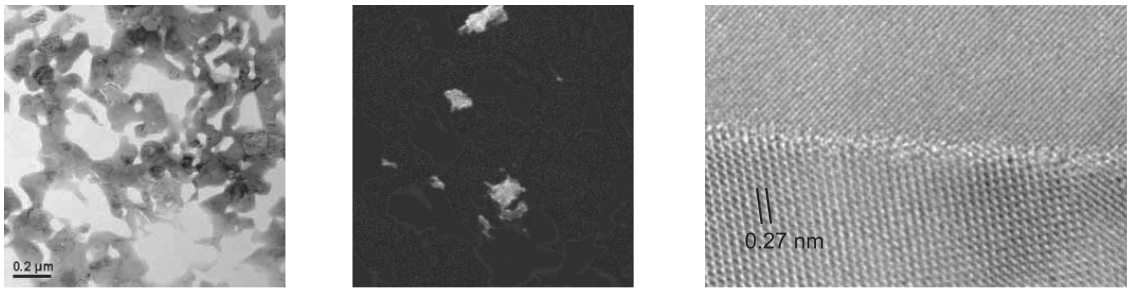


*Fig. 9.* (a) Bright field TEM image and (b) corresponding mapping at Co L-edge of CGO + 5 cat% cobalt oxide sintered at 900°C for 2 h and cooled with −0.5°C/min. (c) High resolution TEM image of CGO + 5 cat% cobalt oxide sintered at 900°C for 2 h and quenched in air showing a disordered grain boundary layer of roughly 0.5 nm thickness.

cobalt oxide. The low activation energy of 0.54 eV points to an electronic conductor. Supporting evidence comes from Koumoto et al. [33], who reported on the DC 4-point conductivity of $Co_3O_4$. They observed an increase in conductivity and also an increasing activation energy from room temperature up to roughly 840°C for $Co_3O_4$. After the transition to CoO, the total conductivity is lower and of constant activation energy. By evaluating their data, this activation energy is calculated as 0.59 eV. The conductivity of $Co_3O_4$ at temperatures <800°C was also measured by Sakamoto et al. [34] and they found a value 0.71 eV. This value is much larger than the one calculated in the present work. Furthermore, the second conductivity mechanism can not be due to an intrinsic grain boundary resistance of CGO10 ceramic. Depending on grain size, the value of the activation energy for grain boundary conductivity lies usually between 1 and 1.2 eV [35]. It is therefore concluded that CoO forms a percolating network at the grain boundaries at temperatures between 900 and 1000°C, which accounts for the increased conductivity in quenched samples with an activation energy of around 0.54 eV.

## Conclusion

The total conductivity of undoped $Ce_{0.9}Gd_{0.1}O_{1.95}$ (CGO10) as well as cobalt oxide doped CGO10 was investigated by DC 4-point conductivity measurements. The addition of up to 5 cat% of cobalt oxide did not change the total conductivity of CGO10 when it was slowly cooled after sintering. Quenched CGO10 however, exhibited an enhanced conductivity at temperatures below 250°C. This additional conductivity with an activation energy of only 0.55 eV is attributed to CoO which is reduced from $Co_3O_4$ at temperatures above 900°C. Furthermore, it could be shown that cobalt oxide can be found in the form of isolated particles in the CGO10 matrix as well as a very thin, but coherent grain boundary layer of 0.5 nm thickness. The cobalt oxide phase forms a percolating network and contributes an additional conductivity mechanism evident at low temperature with electronic charge carriers. The fact that the cooling rate controls the overall conductivity opens interesting possibilites to tailor the electrical response of cobalt oxide doped CGO10 electrolytes.

## Acknowledgment

Prof. G. Günther from the Trace Element and Micro Analysis Group at ETH Zurich is gratefully acknowledged for chemical analysis. Dr. F. Krumeich from the Laboratory of Inorganic Chemistry of ETH Zurich is gratefully acknowledged for the TEM bright field images and the elemental mappings. Dr. Z. Zhang and Dr. W. Sigle from the MPI Stuttgart are kindly acknowledged for the HREM images. Financial support for this research was provided by COST525 and CTI TOP Nano 21 Project No. 5978.2.

## References

1. J. Will, A. Mitterdorfer, C. Kleinlogel, D. Perednis, and L.J. Gauckler, *Solid State Ionics*, **131**, 79 (2000).
2. N.Q. Minh, *J. Am. Ceram. Soc.*, **76**, 563 (1993).
3. M. Goedickemeier and L.J. Gauckler, *J. Electrochem. Soc.*, **145**, 414 (1998).
4. B.C.H. Steele, *Solid State Ionics*, **129**, 95 (2000).

5. D.K. Hohnke, *Solid State Ionics*, **5**, 531 (1981).
6. A. Overs and I. Riess, *J. Am. Ceram. Soc.*, **65**, 606 (1982).
7. J. Faber, C. Geoffroy, A. Roux, A. Sylvestre, and P. Abelard, *Appl. Phys. A-Mater. Sci. Process.*, **49**, 225 (1989).
8. K.Q. Huang, M. Feng, and J.B. Goodenough, *J. Am. Ceram. Soc.*, **81**, 357 (1998).
9. S.R. Wang, T. Kobayashi, M. Dokiya, and T. Hashimoto, *J. Electrochem. Soc.*, **147**, 3606 (2000).
10. V.V. Kharton, F.M. Figueiredo, L. Navarro, E.N. Naumovich, A.V. Kovalevsky, A.A. Yaremchenko, A.P. Viskup, A. Carneiro, F.M.B. Marques, and J.R. Frade, *J. Mater. Sci.*, **36**, 1105 (2001).
11. T.S. Zhang, P. Hing, H.T. Huang, and J. Kilner, *Solid State Ionics*, **148**, 567 (2002).
12. J. Van herle, T. Horita, T. Kawada, N. Sakai, H. Yokokawa, and M. Dokiya, *Solid State Ionics.*, **86–88**, 1255 (1996).
13. P.L. Chen and I.W. Chen, *J. Am. Ceram. Soc.*, **79**, 1793 (1996).
14. P.L. Chen and I.W. Chen, *J. Am. Ceram. Soc.*, **79**, 3129 (1996).
15. C. Kleinlogel and L.J. Gauckler, *Solid State Ionics*, **135**, 567 (2000).
16. G.S. Lewis, A. Atkinson, and B.C.H. Steele, in Fourth European Solid Oxide Fuel Cell Forum, edited by U. Bossel (Oberrohrdorf, Switzerland, 2000), p. 773.
17. C. Kleinlogel and L.J. Gauckler, *Advanced Materials*, **13**, 1081 (2001).
18. G.S. Lewis, A. Atkinson, B.C.H. Steele, and J. Drennan, *Solid State Ionics*, **152**, 567 (2002).
19. D.P. Fagg, J.C.C. Abrantes, D. Perez-Coll, P. Nunez, V.V. Kharton, and J.R. Frade, *Electrochim. Acta*, **48**, 1023 (2003).
20. E. Jud, C.B. Huwiler and L.J. Gauckler, *J. Am. Ceram. Soc.* (in press).
21. E. Jud, C.B. Huwiler, and L.J. Gauckler, submitted to *J. Am. Cer. Soc.*
22. J. Luo, H. Wang, and Y.-M. Chiang, *J. Am. Ceram. Soc.*, **82**, 916 (1999).
23. M.I. Mendelson, *J. Am. Ceram. Soc.*, **52**, 443 (1969).
24. B. Hattendorf, C. Latkoczy, D. Gunther, *Analytical Chemistry*, **75**, 341A (2003).
25. R. Gerhardt and A.S. Nowick, *J. Am. Ceram. Soc.*, **69**, 641 (1986).
26. X.D. Zhou, W. Huebner, I. Kosacki, and H.U. Anderson, *J. Am. Ceram. Soc.*, **85**, 1757 (2002).
27. E. Jud and L.J. Gauckler, *J. Electroceram.*, **14**, 247 (2005).
28. C.M. Kleinlogel and L.J. Gauckler, *J. Electroceram.*, **5**, 231 (2000).
29. K. Mocala, A. Navrotsky, and D.M. Sherman, *Phys. Chem. Miner.*, **19**, 88 (1992).
30. E. Jud and L.J. Gauckler, submitted to J. Electroceram.
31. M. Chen, B. Hallstedt, N.A. Grundy, and L.J. Gauckler, *J. Am. Ceram. Soc.*, **86**, 1567 (2003).
32. N.A. Grundy, private communication (2004).
33. K. Koumoto and H. Yanagida, *Jpn. J. Appl. Phys.*, **20**, 445 (1981).
34. S. Sakamoto, M. Yoshinaka, K. Hirota, and O. Yamaguchi, *J. Am. Ceram. Soc.*, **80**, 267 (1997).
35. G.M. Christie and F.P.F. vanBerkel, *Solid State Ionics*, **83**, 17 (1996).